Geotechnical Engineering in the XXI Century: Lessons learned and future challenges
N.P. López-Acosta et al. (Eds.)

doi:10.3233/STAL190205

Performance Evaluation of a Modified UIUC Model with the Consideration of Principal Stress Axis Rotation

Tianshu LIN[a], Tatsuya ISHIKAWA[b,1], Tetsuya TOKORO[c], Bin LUO[a] and Erol TUTUMLUER[d]
[a]*Graduate School of Engineering, Hokkaido University*
[b]*Faculty of Public Policy, Hokkaido University*
[c]*Department of Engineering of Innovation, National Institute of Technology, Tomakomai College*
[d]*Department of Civil and Environmental Engineering, University of Illinois at Urbana-Champaign*

Abstract. The primary failure mechanism of unbound aggregate materials in flexible pavements is rutting or accumulation of permanent deformation. Basically, permanent deformation of unbound materials is influenced by many factors including stress level, numbers of loading, principal stress axis rotation under moving wheel loading, shear strength, moisture content and so on. Many models, both purely mechanics-based and mechanistic-empirical, have been developed to predict permanent strain accumulation. Purely mechanics-based models are hard to implement in pavement design because they are often complicated and time-consuming in prediction. Mechanistic-empirical models are widely used in pavement design due to fast computation and acceptable accuracy of prediction. The recently developed UIUC model shows good applicability for permanent deformation prediction based on repeated load triaxial tests results often conducted at constant confining pressure. Consequently, the effect of principal stress axis rotation on permanent deformation is not considered. This drawback limits the use of UIUC model in pavement design because the actual principal stress axis rotation due to moving wheels greatly increases permanent deformation. In this study, a modified UIUC model has been proposed based on multi-ring shear tests results, which could simulate principal stress axis rotation in the pavement structure. A new parameter, $(R_s)_{ave}$, is added to capture the effect of principal stress axis rotation on the permanent strain. This modified UIUC model shows good applicability to predict permanent axial strains of crusher-run materials studied in laboratory testing for the effects of principal stress axis rotation and moisture.

Keywords. Principal stress axis rotation, unbound aggregate, rutting.

1. Introduction

Numerous studies have been conducted to investigate effects of principal stress axis rotation on mechanical properties of soils, which is routinely encountered in pavement engineering due to moving wheel loads. Most of these studies have considered Hollow

[1] Corresponding Author, Faculty of Engineering, Hokkaido University, Hokkaido, Japan; E-mail: t-ishika@eng.hokudai.ac.jp.

Cylinder Apparatus (HCA) testing. However, most of them use a loading stress path such that the angle of principal stress axis rotation is always positive and the direction of major principal stress usually increases from zero to 180° [1-6]. In other words, the major principal stress always rotates counterclockwise. On the other hand, with shear stress reversals, the direction of major principal stress may constantly oscillate between positive and negative values, and this is a critical issue to study for pavement materials [7].

Ishikawa et al. [8] developed a multi-ring shear apparatus for laboratory element tests, which could apply cyclic axial load and shear stress. One great advantage of multi-ring shear apparatus is that it allows simulating principal stress axis rotation with stress reversal simply by applying cyclic axial stress and shear stress simultaneously. This study uses test results obtained from multi-ring shear apparatus to investigate the principal stress rotations and check the applicability of a modified UIUC model [9].

2. Test apparatus

The schematic diagram of the multi-ring shear apparatus is shown in Figure 1 (a). The terms regarding size (H, W, α), load, stress, and strain used in multi-ring shear apparatus are defined as shown in Figure 1 (b). The width of the specimen is 60 mm and the height is 60 mm. Two types of cyclic loading tests were performed as cyclic axial loading test and cyclic axial and shear loading test. In cyclic axial loading test, a sinusoidal waveform axial load, similar to repeated loading triaxial test without rotation of the principal stress axis, is applied. In this research, the cyclic axial tests are referred to as fixed-place loading tests (FL tests). In cyclic axial and shear loading test, the sinusoidal waveform axial load and the shear load are cyclically applied on the specimen. The shear load is cyclically applied in a bidirectional way (simulating two-way traffic on the pavement) by changing the phase angle of 180° for every succeeding loading cycle. This test is considered as a moving-wheel loading simulation (ML tests) in which the rotation of the principal stress axis occurs similar to in-situ traffic loading conditions. The number of loading cycles applied in both FL and ML tests is 400.

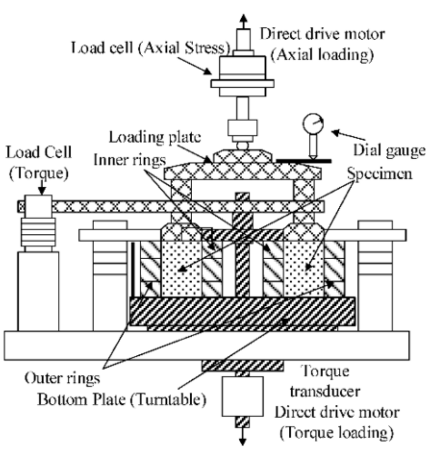

(a) Multi-ring shear apparatus

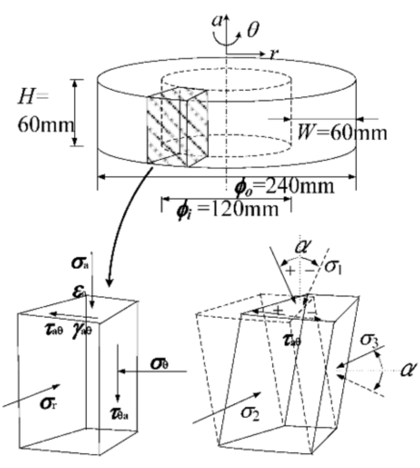

(b) Definition of stress and deformation

Figure 1. Test apparatus and definition of stress and deformation. (after Ishikawa et al., [10]).

As this apparatus applies both axial stress and shear stress directly, principal stresses can be calculated through Eqs. (1) to (4).

$$\sigma_1 = \frac{\sigma_a + K_0\sigma_a}{2} + \frac{\sqrt{(\sigma_a - K_0\sigma_a)^2 + 4{\tau_{a\theta}}^2}}{2} \tag{1}$$

$$\sigma_2 = K_0\sigma_a \tag{2}$$

$$\sigma_3 = \frac{\sigma_a + K_0\sigma_a}{2} - \frac{\sqrt{(\sigma_a - K_0\sigma_a)^2 + 4{\tau_{a\theta}}^2}}{2} \tag{3}$$

$$K_0 = 1 - \sin\phi' \tag{4}$$

where K_0 is coefficient of earth pressure at rest; ϕ' is effective internal friction angle; σ_a is applied axial stress; $\tau_{a\theta}$ is applied shear stress.

The values of the effective friction angle are listed in Table 1 as calculated by Inam [11]. Materials used in this research include a natural crusher-run with 9.5 mm maximum particle size (C-9.5) and recycled crusher-run which is obtained from the demolished concrete structure with a 9.5 mm maximum particle size (RC-9.5). Inam [11] performed a series of monotonic and cyclic loading tests. The field data [12] show that the degree of saturation (S_r) of the unbound base course material in Hokkaido lies in the range of 20 % to 50 % throughout the year. Consequently, S_r of the specimen was selected as 19%, 33%, and 48%. An oven-dried sample was also selected to compare the results with those of the unsaturated specimen. A dry density in the range of 1.581–1.583 g/cm^3 was selected for the multi-ring shear tests, which is about 90% of the maximum dry density. The stress states for the multi-ring shear tests were determined based on a stress analysis of a Japanese paved road model by the General Analysis Multi-layered Elastic Systems (GAMES) [13]. The maximum axial load and shear stress applied are 114.2 kPa and 30 kPa, respectively. To check the effect of principal stress axis rotation, another set of ML tests was performed on the C-9.5 material with a maximum applied shear stress of 15 kPa.

Table 1. ϕ' and K_0 and of test materials.

Test material	**Degree of saturation, S_r (%)**	**Effective internal friction angle, ϕ' (deg.)**	**Coefficient of earth pressure at rest, K_0**
C-9.5	oven-dried	21.6	0.63
	19%	14.7	0.75
	33%	17.4	0.70
	48%	18.4	0.68
RC-9.5	oven-dried	18.1	0.69
	19%	-	-
	33%	16.3	0.72
	48%	17.0	0.70

As the effective friction angle varies with moisture content, the value of K_0 also varies with moisture content. As a result, the principal stresses also vary with moisture content. To clearly show the level of principal stress axis rotation, three parameters could be calculated as the direction of major principal stress (Eq. (5)), stress ratio (Eq. (6)), and principal stress parameter (Eq. (7)).

$$\alpha = \sin^{-1}\sqrt{\frac{\sigma_2 - \sigma_3}{\sigma_1 - \sigma_3}} \tag{5}$$

$$\eta = \frac{q}{p'} \tag{6}$$

$$b = \frac{\sigma_2 - \sigma_3}{\sigma_1 - \sigma_3} \tag{7}$$

where η is stress ratio, which is composed of two stress invariants, mean normal stress, p', and deviator stress, q. b is the principal stress parameter, which describes the relative magnitudes of the three principal stresses. α is the angle of principal stress axis rotation. Mean normal stress, p', and deviator stress, q, are calculated through Eqs. (8) and (9).

$$p' = \frac{\sigma_1 + \sigma_2 + \sigma_3}{3} \tag{8}$$

$$p' = \frac{\sigma_1 + \sigma_2 + \sigma_3}{3} \tag{9}$$

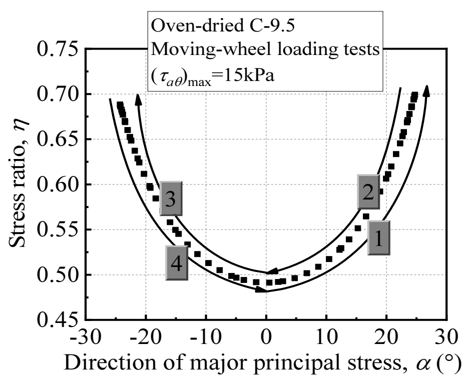

Figure 2. Stress ratios and directions of major principal stress axis applied during ML test.

Figure 2 shows the relationship between the direction of major principal stress, α, and stress ratio, η, during ML testing of oven-dried C-9.5. α is calculated through Eq. (5) and it represents the angle of principal stress axis rotation. Figure 1 (b) illustrates the definition of α. As shown in Figure 2, α oscillates between positive and negative values during one loading but does not increase monotonically and this phenomenon is stress reversal. To be specific, α increases from zero to the maximum value (about 25°) in stage 1 and then decreases to zero in stage 2. After that, α decreases continually to the minimum value (about -25°) in stage 3 and finally goes back to zero in stage 4. As mentioned before, stress reversals caused by moving wheel loads are critical for the long-term satisfactory pavement performance and this apparatus could reproduce this phenomenon well.

3. Modified UIUC model

Though the level of principal stress axis rotation could be captured through these three parameters, this method is hard to use in practice as the calculation is complex. To capture the effect of principal stress axis rotation on permanent deformation, a parameter, $(R_s)_{\text{ave}}$, proposed by Ishikawa et al. [10,14] is used. $(R_s)_{\text{ave}}$ is the average ratio of axial strains considered with and without principal stress axis rotation in the specimen. Besides, $(R_s)_{\text{ave}}$ could be roughly approximated by Eq. (10). Adding Eq. (10) to the UIUC model [15], the permanent deformation of unbound pavement materials under repeated moving wheel loads could be predicted [9]. The modified UIUC model is defined in Eq. (11).

$$(R_s)_{\text{ave}} = \exp\left(E\frac{(\tau_{a\theta})_{\max}}{(\sigma_a)_{\max}}\right) \tag{10}$$

where $(\tau_{a\theta})_{\max}$ is maximum of applied shear stress; $(\sigma_a)_{\max}$ is maximum applied axial stress; E is a regression parameter.

$$\varepsilon_p(N) = AN^B\left(\frac{(\sigma_a)_{\max}}{p_a}\right)^C\left(\frac{p_a}{\tau_{\max}}\right)^D\exp\left(E\frac{(\tau_{a\theta})_{\max}}{(\sigma_a)_{\max}}\right) \tag{11}$$

where $\varepsilon_p(N)$ is permanent strain corresponding to N-load applications; N is number of load cycles; $\tau_{\max}$ is shear strength, which is estimated through monotonic shearing test [9]; p_a is the atmospheric pressure, equals to 101 kPa in this study; A to E are regression parameters.

To check the applicability of the newly added parameter, the value of $(R_s)_{\text{ave}}$ is determined by calculating the average ratio of axial strains obtained in the specimen with and without principal stress axis rotation considered. Then, the value of parameter E could be derived through Eq. (10). The values of other parameters, A, B, C, D, in Eq. (11) are obtained through a regression analysis of test results without principal stress axis rotation (FL test) as shown in Table 2 and Figure 3. Owing to the synergistic effects of principal stress axis rotation and change in moisture content, it is necessary to conduct regression analyses separately for test results with different shear stress amplitudes, though Eq. (10) could capture the effect of shear stress amplitude. Besides, previous research [10] pointed out that effect of moisture content could be fully captured by shear strength when there is no principal stress axis rotation. However, the synergistic effect of principal stress axis rotation and change in moisture content indicates that $(R_s)_{\text{ave}}$ is another parameter that reflects the effect of moisture content. More details of this synergistic effect are discussed in the next section.

Table 2. Results of regression analyses using the modified UIUC model.

Test materials	Test types	A in Eq. (11)	B in Eq. (11)	C in Eq. (11)	D in Eq. (11)	$(R_s)_{\text{ave}}$	E in Eq. (10)	R^2	RMSE	E in Eq. (11)	R^2	RMSE
C-9.5	FL	0.552	0.128	1.318	0.782	-	-	0.951	0.059	-	0.951	0.059
	ML (15kPa)	0.552	0.128	1.318	0.782	2.09	5.612	0.909	0.212	5.610	0.910	0.213
	ML (30kPa)	0.552	0.128	1.318	0.782	2.87	4.008	0.851	0.484	3.772	0.866	0.460
RC-9.5	FL	0.994	0.091	0.689	0.870	-	-	0.932	0.097	-	0.932	0.097
	ML (30kPa)	0.994	0.091	0.689	0.870	2.21	3.016	0.914	0.327	2.914	0.922	0.310

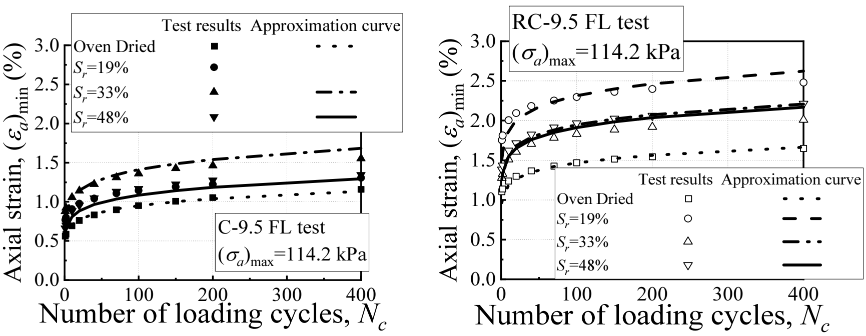

(a) C-9.5 (b) RC-9.5

Figure 3. Estimation of the permanent axial strain in FL tests.

The trend of permanent deformation accumulation of unbound pavement materials under repeated moving wheel loads could be drawn through substituting values of A to E into Eq. (11). As shown in Figure 4 and Table 2, the R^2 is high enough to demonstrate the applicability of the modified model. As a supplement to the R^2, the value of Root Mean Square Error (RMSE) is also calculated. The value of RMSE is also low enough to validate the accuracy of this model. In other words, specimens with and without principal stress axis rotation have the same value of A to D when other test conditions are same. The principal stress axis rotation conditions amplify the permanent deformation. Besides the principal stress axis rotation, the permanent deformation is also affected by the material physical properties. As shown in Table 2, RC-9.5 has a smaller value of $(R_s)_{ave}$ than that of C-9.5, which implies that principal stress axis rotation has a much more significant effect on C-9.5 than RC-9.5. Noted that there are only three approximation lines but not four for C-9.5, the curve of S_r=19% is excluded. C-9.5 with 19% degree of saturation has the lowest shear strength and it should have the largest deformation. However, permanent deformation of C-9.5 with S_r=19% is only larger than that of S_r=33% as shown in Figure 3 (a). This phenomenon may be due to an experimental error. For example, the suction cannot be controlled in this apparatus and the uniformity of water may not be ensured.

Besides, the value of parameter E could also be determined from regression analysis through the use of Eq. (11). The values of parameter E in this method are also listed in Table 2. The E values in Eq. (10) and Eq. (11) are almost similar, which indicates the applicability of the newly added parameter, $(R_s)_{ave}$.

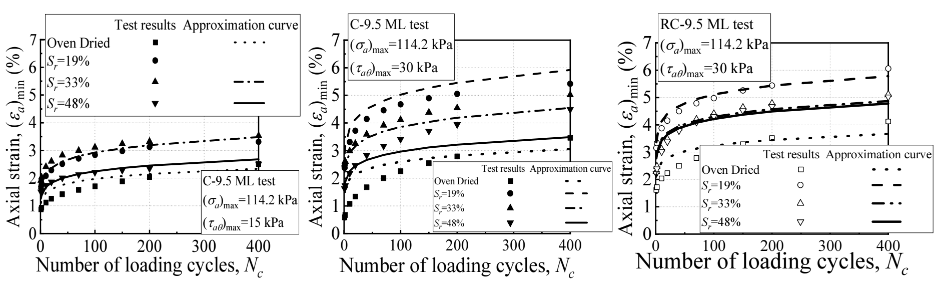

(a) C-9.5 ($(\tau_{a\theta})_{max}$ =15 kPa) (b) C-9.5 ($(\tau_{a\theta})_{max}$ =30 kPa) (c) RC-9.5

Figure 4. Estimation of the permanent axial strain in ML tests.

4. Effects of principal stress axis rotation

As mentioned before, the effective friction angle and K_0 vary with moisture content. As a result, the principal stresses and three parameters also vary with moisture content. It is reasonable to conclude that, the effect of principal stress axis rotation is also influenced by moisture content.

Figure 5 shows how moisture content affects the direction of major principal stress. It is noted that the sequence of η from high to low is oven-dried, S_r=48%, S_r=33%, S_r=19% when other test conditions are same. Besides, this sequence is also the narrowest amplitude of α to widest. Moreover, as shown in Figure 4, this sequence of the smallest permanent strain to the largest is same as oven-dried, S_r=48%, S_r=33%, S_r=19%. As a result, it is reasonable to conclude that η and α are affected by moisture content when test material and applied stress are same. Moreover, the greater α, the greater the permanent strain.

As shown in Figure 6 (a), increasing shear stress amplitude from 15 kPa to 30 kPa, the magnitudes of α for specimens with different moisture contents becomes similar and the value of E decreases, which implies that the effect of moisture content on α is also influenced by the stress state. To be specific, α for specimens with different moisture contents varies from 24.74° to 30.16° with 15 kPa shear stress amplitude whereas it only varies from 33.48° to 36.86° with 30 kPa shear stress. As shown in Figure 6 (b), the value of E in Eq. (11) has a positive relation with increment of α (difference between maximum and minimum α under the same shear stress amplitude). Consequently, a smaller E equals to a smaller range of α, which indicates that the synergistic effect of principal stress axis rotation and change in moisture content is less significant at higher shear stress amplitude.

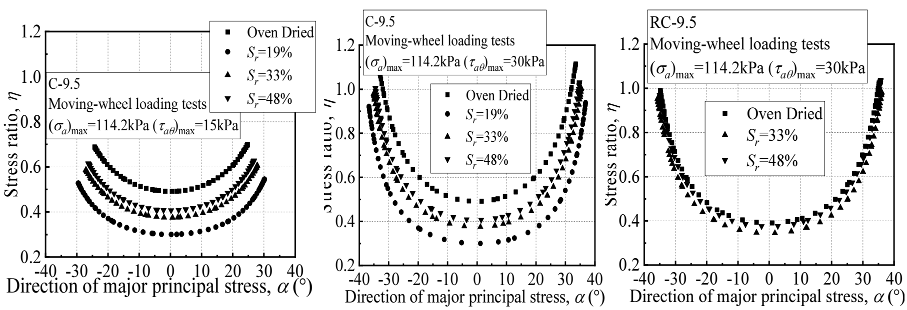

(a) C-9.5 ML test ($(\tau_{a\theta})_{max}$ =15 kPa) (b) C-9.5 ML test ($(\tau_{a\theta})_{max}$ =30 kPa) (c) RC-9.5 ML test ($(\tau_{a\theta})_{max}$ =30 kPa)

Figure 5. Stress paths analyzed.

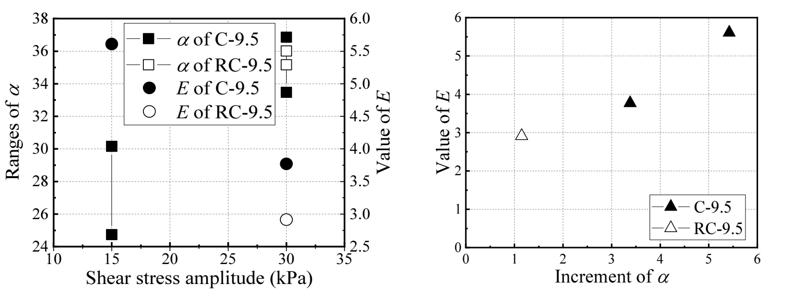

(a) Relation between shear stress amplitude and α (b) Relation between E and increment of α

Figure 6. Synergistic effect of principal stress axis rotation and change in moisture content.

5. Conclusions

This study investigated the applicability of a modified UIUC model for predicting laboratory specimen permanent axial strain accumulation by considering principal stress axis rotation. Following conclusions are obtained:

- Principal stress axis rotation greatly amplifies the accumulation of permanent deformations and a newly added model variable, $(R_s)_{ave}$, could easily capture this effect of principal stress axis rotation simulating moving wheel load effects.
- By measuring the stress ratio and direction of major principal stress, the level of principal stress axis rotation could be estimated, and this level was affected by moisture content. The synergistic effect of principal stress axis rotation and change in moisture content was less significant with higher shear stress amplitude.
- The modified UIUC model showed good applicability for predicting permanent deformation trends of unbound aggregates with principal stress axis rotation.

These findings need further validation as they are obtained through two types of crusher-run materials, and the applied axial load and shear stress are limited. Further, more comprehensive future studies should consider including additional pavement materials and applied stress conditions to further validate the findings presented herein.

Acknowledgements

This research was supported in part by Grant-in-Aid for Scientific Research (C) (18560479) and (B) (20360206) from Japan Society for the Promotion of Science (JSPS) KAKENHI. The authors also acknowledge the support by China Scholarship Council.

References

[1] Al-Rkaby, A. H., Chegenizadeh, A., & Nikraz, H. R. (2017). "Cyclic behavior of reinforced sand under principal stress rotation", *Journal of Rock Mechanics and Geotechnical Engineering*, 9(4): 585-598.

[2] Tong, Z. X., Zhang, J. M., Yu, Y. L., & Zhang, G. (2010). "Drained deformation behavior of anisotropic sands during cyclic rotation of principal stress axes", *Journal of Geotechnical and Geoenvironmental Engineering*, 136(11): 1509-1518.

[3] Wang, Y., Wu, D., Qiu, Y., & Wang, D. (2017). "Experimental investigation on cyclic deformation behavior of soft marine clay involved principal stress rotation", *Marine Georesources & Geotechnology*, 35(4): 571-577.

[4] Yu, H. S., Yang, L. T., Li, X., & Wanatowski, D. (2016). "Experimental investigation on the deformation characteristics of granular materials under drained rotational shear", *Geomechanics and Geoengineering*, 11(1): 47-63.

[5] Xiong, H., Guo, L., Cai, Y., & Yang, Z. (2016). "Experimental study of drained anisotropy of granular soils involving rotation of principal stress direction", *European Journal of Environmental and Civil Engineering*, 20(4): 431-454.

[6] Nakata, Y., Hyodo, M., Murata, H., & Yasufuku, N. (1998). "Flow deformation of sands subjected to principal stress rotation", *Soils and Foundations*, 38(2): 115-128.

[7] Brown, S. F. (1996). "Soil mechanics in pavement engineering", *Géotechnique*, 46(3): 383-426.

[8] Ishikawa, T., Miura, S., & Saeki, E. (2007). "Development performance evaluation of multi-ring shear apparatus", *Design and Construction of Pavement and Rail Track*, 53-64.

[9] Ishikawa, T., Lin, T., Yang, J., Tokoro, T., & Tutumluer, E. (2019). "Application of the UIUC model for predicting ballast settlement to unsaturated ballasts under moving wheel loads", *Transportation Geotechnics*, 18: 149-162.

[10] Ishikawa, T., Sekine, E., & Miura, S. (2011). "Cyclic deformation of granular material subjected to moving-wheel loads", *Canadian Geotechnical Journal*, 48(5): 691-703.
[11] Inam, A. (2012). "Performance evaluation of unsaturated base course materials subject to repeated traffic loads", Hokkaido University.
[12] Ishikawa, T., Kawabata, S., Kameyama, S., Abe, R. & Ono, T. (2012). "Effects of freeze-thawing on mechanical behavior of granular base in cold regions", Proceedings of the 2nd International Conference on Transportation Geotechnics (ICTG), Sapporo, Japan, 118-124.
[13] Maina, J., & Matsui, K. (2004). "Developing software for elastic analysis of pavement structure responses to vertical and horizontal surface loadings", *Transportation Research Record: Journal of the Transportation Research Board*, (1896): 107-118.
[14] Ishikawa, T., Miura, S., & Sekine, E. (2014). "Simple plastic deformation analysis of ballasted track under repeated moving-wheel loads by cumulative damage model", *Transportation Geotechnics*, 1(4): 157-170.
[15] Chow, L.C., and Mishra, D., and Tutumluer, E. (2014). "Framework for Improved Unbound Aggregate Base Rutting Model Development for Mechanistic-Empirical Pavement Design", *Transportation Research Record*, (2401): 11-21.